

DETECTION AND ISOLATION OF LEAKAGE AND VALVE FAULTS IN HYDRAULIC SYSTEMS IN VARYING LOADING CONDITIONS, PART 2: FAULT DETECTION AND ISOLATION SCHEME

Jarmo Nurmi and Jouni Mattila

*Tampere University of Technology, Department of Intelligent Hydraulics and Automation
P.O. Box 589, 33101 Tampere, Finland
jarmo.nurmi@tut.fi*

Abstract:

Leakages and valve faults are among the most common faults in hydraulic systems. This paper studies the real-time detection and isolation of certain leakage and valve faults based on the results obtained in part one. In the first part, the mathematical model of a hydraulic test bed was analysed with Global Sensitivity Analysis to facilitate a systematic and verified approach to model-based condition monitoring. In this paper, an Unscented Kalman Filter-based Fault Detection and Isolation scheme for leakage and valve faults of a generic servo valve-controlled hydraulic cylinder is devised. Compared to existing literature, the leakage and valve faults are decoupled from cylinder static and dynamic loading which makes the results generic and applicable to any servo valve-controlled hydraulic cylinder. Moreover, a more comprehensive set of fault patterns for the detection and isolation of leakages and valve faults with experimental and simulation results are presented. We show that detecting an external leakage of as small as 0.17 l/min is possible in some cases, but the accuracy of the method varies considerably. We also report why the isolation of valve faults from leakages is very difficult.

Keywords: fault detection and isolation, leakages, valve faults, varying load, unscented kalman filter, fault patterns

1 Introduction

The idea of model-based condition monitoring is to create a model output $\hat{y}(k)$, which is subtracted from actual measurement $y(k)$ to create a residual $r(k)$ revealing the health of the system (Isermann, 2006). If the model is ideal, the residual remains at zero when the system is operating correctly. But when a fault is introduced, the residual deviates from zero, which is noticed by the fault detection process. Then the fault isolation process takes over and localizes the cause of the fault. The scheme as a whole is called Fault Detection and Isolation (FDI), see Fig. 1.

In practice, measurements are noisy and perfect plant models are not possible. Therefore discrepancy between measured and modelled outputs is to be expected. For this reason state estimators (or Kalman Filters) which can consider modelling errors, measurement noise, and utilize measurements to correct model predictions are common in condition monitoring (An et al., 2008; Sepasi et al., 2010).

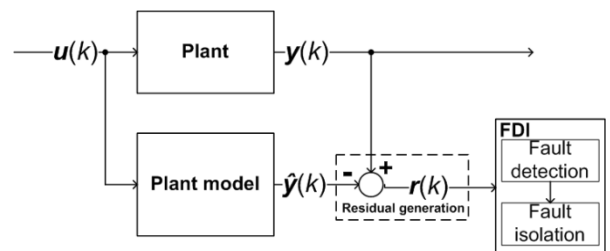


Fig. 1: The model-based FDI scheme

Previously, An and Sepehri (2008) proposed a method using a fault-free Extended Kalman Filter (EKF) to detect leakages with actuators under unknown external loading. Using the EKF to estimate the external force, they showed that external leakages out of the system and internal leakages across cylinder chambers as small as 0.25 l/min could be detected and isolated. Their approach was proven to work well with sinusoidal and fairly well with pseudorandom inputs.

This manuscript was received on 4 March 2011 and was accepted after revision for publication on 27 September 2011

More recently, Sepasi and Sassani (2010) applied the Unscented Kalman Filter (UKF) to detect leakages and load changes from a hydraulic system with a constant, known external force. They could detect and isolate leakage faults and load changes. However, results were provided using only sinusoidal inputs.

Chen (2010) devised a scheme to detect and isolate internal leakage and sensor offsets. The possibility of decoupling external force from state equations by considering velocity as an input was also proved.

Tan and Sepehri (2002) used the parameters of a nonlinear Volterra model to detect and isolate internal leakage, external leakage, incorrect supply pressure, and contamination in the fluid. Experimental results on the detection of incorrect supply pressure were shown, but the method was offline, which hampers its use for early fault detection. A similar issue affects the fault detection system by Le et al. (1998) where a neural network approach was shown to be sensitive to relatively high leakages of over 1 l/min.

As opposed to model-based approaches, the use of the wavelet transform by Goharrizi et al. (2010a, 2010b) has produced good results by allowing the detection of an internal leakage of 0.124 l/min. But when external leakages were considered in Goharrizi et al. (2011), it was reported that external leakages of 0.30 l/min could be isolated from an internal leakage of 0.48 l/min, and furthermore external leakages cannot be localized to either side of the actuator, which has been proven to be possible with model-based approaches (An et al., 2008).

In this paper, we extend the methods of Sepasi and Sassani (2010) and An and Sepehri (2008) by treating a more extensive set of faults than those papers and adopting a similar method as Chen (2010) to obtain independence from varying load. The latter is possible as we have a sufficient quality position measurement from which we differentiate velocity, which eliminates the need to estimate them. Thus, we do not need to know the external force nor the load mass, as the information of the mechanism is included in the position and velocity measurement. Therefore, this scheme is more viable in generic hydraulic systems where the load can vary during operation. This paper utilizes the model and Global Sensitivity Analysis (GSA) that was presented for our test bed in (Nurmi and Mattila, 2011). This combines into a systematic approach to model-based condition monitoring compared to the ad hoc approaches currently present. An adaptive threshold is also proposed and experimental results are given with random control signals that are more plausible than sinusoidal inputs. The paper focuses on common leakage and valve faults (Watton, 2007).

This paper is organized as follows. In Section 2, the applicability of the method and the test bed are briefly discussed. In Section 3, the UKF algorithm is introduced and the reduced-order UKF is applied to the test bed. In Section 4, the capability of the UKF and the adaptive threshold scheme are experimentally tested in detecting and isolating leakages and with simulations in detecting and isolating valve faults.

2 Applicability of the Scheme and Test Bed

As shown in Fig. 2, the FDI scheme used in this paper is applicable to a generic valve-controlled hydraulic cylinder that drives any of the n-DOF manipulator joints affected by any external force and inertia load. The scheme is considered to be suitable especially for detecting and isolating external and internal leakages.

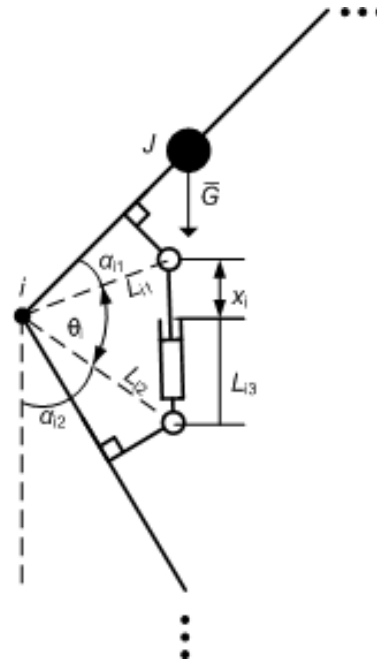


Fig. 2: A manipulator joint driven by a hydraulic cylinder

2.1 Test Bed

As a case study to experimentally validate the scheme, the test bed, in Fig. 3 and Fig. 4, is used in leakage fault study. It has a 4/3-directional valve that controls the joint cylinder, and three restrictor valves which emulate external leakages between the cylinder and the directional valve ('External leakage A' and 'External leakage B') and internal leakage across cylinder chambers ('Internal leakage'), for a list of system components see (Nurmi and Mattila 2011).

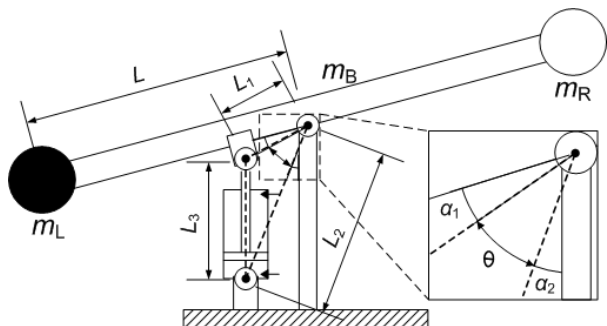


Fig. 3: Illustration of the test bed

In (Nurmi and Mattila, 2011), the model and GSA of the test bed were presented. In this paper, we use that model to simulate valve faults and utilize the GSA results in the verification of the UKF process model and in the development of the fault detection scheme.

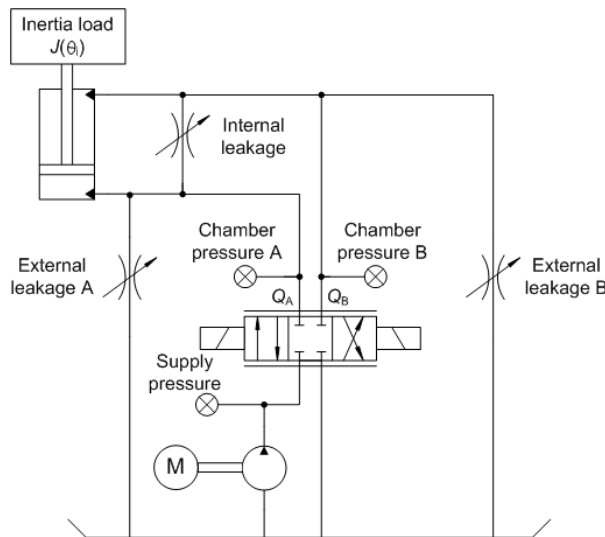


Fig. 4: The hydraulic diagram of the test bed

3 Unscented Kalman Filter

In this section, an UKF scheme is devised to facilitate model-based FDI. The basis for the scheme originates from Sepasi and Sassani (2010) and An and Sephri (2008). However, neither scheme is directly applicable to a generic hydraulic system where the load force and mass are not constant or known. Therefore, a modified version is used with decoupling of external force and load mass similar to (Chen, 2010).

This section is organized as follows. In Section 3.1, a generic discrete nonlinear system and its state estimation are introduced. Then in Section 3.2, the UKF algorithm is presented and implemented for the test bed in Section 3.3. Fault detection and isolation principles are discussed in Sections 3.4 to 3.5.

3.1 Discrete Nonlinear System with Noise and State Estimation

The system is discrete with a nonlinear process f and measurement model h with noise vectors w and v :

$$\begin{aligned} \mathbf{x}_{k+1} &= f(\mathbf{x}_k, \mathbf{u}_k, t_k) + \mathbf{w}_k \\ \mathbf{y}_{k+1} &= h(\mathbf{x}_{k+1}, t_k) + \mathbf{v}_{k+1} \end{aligned} \quad (1)$$

where \mathbf{x} is a $N \times 1$ state vector in which N is the number of states, \mathbf{u} is a $U \times 1$ control vector in which U is the number of controls, t is the time, \mathbf{w} is a $N \times 1$ process noise vector, \mathbf{y} is a $M \times 1$ measurement vector in which M is the number of measurements, \mathbf{v} is a $M \times 1$ measurement noise vector and k is a previous time instant.

The process noise \mathbf{w}_k and measurement noise \mathbf{v}_{k+1} are assumed to be Gaussian, (\mathcal{N}) white (uncorrelated) and additive with zero mean and covariances \mathbf{Q}_k and \mathbf{R}_{k+1} with distributions:

$$\begin{aligned} \mathbf{w}_k &\sim \mathcal{N}(0, \mathbf{Q}_k) \\ \mathbf{v}_{k+1} &\sim \mathcal{N}(0, \mathbf{R}_{k+1}) \end{aligned} \quad (2)$$

Hydraulic measurements can be noisy, pressures especially. Considering the noise in the state estimator ensures that residuals are closer to zero in the fault-free

situation, hence improving fault detection.

A Kalman-type state estimator for the nonlinear system in Eq. 1 is (Welch and Bishop, 2001):

$$\begin{aligned} \hat{\mathbf{x}}_{k+1} &= f(\hat{\mathbf{x}}_k, \mathbf{u}_k, t_k) + K_{k+1} (\mathbf{y}_{k+1} - \hat{\mathbf{y}}_{k+1}) \hat{\mathbf{y}}_{k+1} \\ &= h(\hat{\mathbf{x}}_{k+1}, t_k) \end{aligned} \quad (3)$$

where $\hat{\mathbf{x}}$ is the state estimate vector of size $(N - A) \times 1$ with the positive integer A denoting order-reduction. The innovation gain K_{k+1} is chosen to minimize the mean squared error $E[(\mathbf{x}_{k+1} - \hat{\mathbf{x}}_{k+1})^2]$. The optimal gain is derived in Simon (2006, pp. 318 - 320).

Nonlinear state estimation has no optimal solution since the innovation gain is dependent on covariance which are hard to accurately recover after the states are transformed through nonlinear functions. The non-optimal EKF circumvents the problem of nonlinearity by linearizing nonlinear functions around the previous states so that linear estimation techniques from the Kalman Filter (KF) can be applied. However, in the process it introduces approximation errors depending on the severity of the nonlinearity in functions f and h .

An approach for tackling the problems of the EKF is the UKF, published by Julier et al. (1995). In (Julier and Uhlmann, 1997; Wan and van der Merwe, 2000) it is shown that the UKF approximates the true mean and covariance of the states more accurately than the EKF with Unscented Transformation (UT). The UT approximates the state distribution with deterministically chosen sigma points assuming that state variables are normally distributed.

Besides the accuracy advantage of UKF over EKF, UKF is also derivative-free, which is useful since calculating and writing long derivatives is error-prone. The given advantages motivate the choice of UKF.

3.2 Unscented Kalman Filter Algorithm

The recursive UKF algorithm can be described in a step by step manner as follows (Wan & van der Merwe 2000):

1. Initialize the filter, Eq. 4
2. Estimate the a priori state vector $\hat{\mathbf{x}}_{k+1}^-$ (prediction)
 - a) Generate sigma points around the previous estimate, Eq. 5
 - b) Propagate the sigma points through the nonlinear functions, Eq. 6
 - c) Calculate the state mean, Eq. 7
3. Calculate the a priori error covariance \mathbf{P}_{k+1}^- , Eq. 8
4. Estimate the a posteriori state vector $\hat{\mathbf{x}}_{k+1}^-$
 - a) Unscented transformation for measurements (mean and covariance), Eq. 9
 - b) Calculate the cross-covariance between predicted states and measurements, Eq. 10
 - c) Calculate the Kalman gain, Eq. 11
 - d) Update state estimate, Eq. 12
5. Calculate the a posteriori error covariance \mathbf{P}_{k+1} , Eq. 13
6. Return to step 2

Step 1 is executed once and steps 2 to 6 are repeated. Steps 2 and 3 constitute the first UT, and step

4a the second. The steps correspond to the following equations:

$$\begin{aligned}\hat{\mathbf{x}}_0 &= E(\mathbf{x}_0) \\ \mathbf{P}_0 &= E\left[(\mathbf{x}_0 - \hat{\mathbf{x}}_0)(\mathbf{x}_0 - \hat{\mathbf{x}}_0)^\top\right] \\ k &= 0\end{aligned}\quad (4)$$

$$\begin{aligned}\hat{\mathbf{x}}_k^{(0)} &= \hat{\mathbf{x}}_k \\ \hat{\mathbf{x}}_k^{(i)} &= \hat{\mathbf{x}}_k + \tilde{\mathbf{x}}^{(i)}, \quad i = 1, 2, 3, \dots, 2N \\ \tilde{\mathbf{x}}^{(i)} &= \left(\sqrt{(L + \lambda)\mathbf{P}_k}\right)_i^\top, \quad i = 1, 2, 3, \dots, N\end{aligned}\quad (5)$$

$$\begin{aligned}\tilde{\mathbf{x}}^{(i)} &= -\left(\sqrt{(L + \lambda)\mathbf{P}_k}\right)_i^\top, \quad i = N + 1, \dots, 2N \\ \hat{\mathbf{x}}_{k+1}^{(i)} &= f\left(\hat{\mathbf{x}}_k^{(i)}, u_k, t_k\right)\end{aligned}\quad (6)$$

$$\begin{aligned}w_{(\text{mean})}^{(0)} &= \frac{\lambda}{L + \lambda} \\ w_{(\text{mean})}^{(i)} &= \frac{1}{2(L + \lambda)}, \quad i = 1, 2, 3, \dots, 2N\end{aligned}\quad (7)$$

$$\hat{\mathbf{x}}_{k+1}^- = \sum_{i=0}^{2N} w_{(\text{mean})}^{(i)} \hat{\mathbf{x}}_{k+1}^{(i)}$$

$$\begin{aligned}w_{(\text{cov})}^{(0)} &= \frac{\lambda}{L + \lambda} + (1 - \alpha^2 + \beta) \\ w_{(\text{cov})}^{(i)} &= \frac{1}{2(L + \lambda)}, \quad i = 1, 2, 3, \dots, 2N\end{aligned}\quad (8)$$

$$\mathbf{P}_{k+1}^- = \sum_{i=0}^{2N} w_{(\text{cov})}^{(i)} \left(\hat{\mathbf{x}}_{k+1}^{(i)} - \hat{\mathbf{x}}_{k+1}^-\right) \left(\hat{\mathbf{x}}_{k+1}^{(i)} - \hat{\mathbf{x}}_{k+1}^-\right)^\top + \mathbf{Q}_k$$

$$\begin{aligned}\hat{\mathbf{y}}_{k+1}^{(i)} &= \mathbf{h}\left(\hat{\mathbf{x}}_{k+1}^{(i)}, u_k, t_k\right) \\ \hat{\mathbf{y}}_{k+1} &= \sum_{i=0}^{2N} w_{(\text{mean})}^{(i)} \hat{\mathbf{y}}_{k+1}^{(i)}\end{aligned}\quad (9)$$

$$\mathbf{P}_{yy} = \sum_{i=0}^{2N} w_{(\text{cov})}^{(i)} \left(\hat{\mathbf{y}}_{k+1}^{(i)} - \hat{\mathbf{y}}_{k+1}\right) \left(\hat{\mathbf{y}}_{k+1}^{(i)} - \hat{\mathbf{y}}_{k+1}\right)^\top + \mathbf{R}_{k+1}$$

$$\mathbf{P}_{xy} = \sum_{i=0}^{2N} w_{(\text{cov})}^{(i)} \left(\hat{\mathbf{x}}_{k+1}^{(i)} - \hat{\mathbf{x}}_{k+1}^-\right) \left(\hat{\mathbf{y}}_{k+1}^{(i)} - \hat{\mathbf{y}}_{k+1}\right)^\top \quad (10)$$

$$\mathbf{K}_{k+1} = \mathbf{P}_{xy} \mathbf{P}_{yy}^{-1} \quad (11)$$

$$\hat{\mathbf{x}}_{k+1} = \hat{\mathbf{x}}_{k+1}^- + \mathbf{K}_{k+1} (\mathbf{y}_{k+1} - \hat{\mathbf{y}}_{k+1}) \quad (12)$$

$$\mathbf{P}_{k+1} = \mathbf{P}_{k+1}^- - \mathbf{K}_{k+1} \mathbf{P}_{yy} \mathbf{K}_{k+1}^\top = \mathbf{P}_{k+1}^- - \mathbf{P}_{xy} \mathbf{P}_{yy}^{-1} \mathbf{P}_{xy}^\top \quad (13)$$

where E is the expectation operator, w is a weighting coefficient, L is the dimension of the state vector and λ is a scaling parameter, satisfying $\lambda = \alpha^2 (L + \kappa) - L$. The parameter α is a tuning factor which determines the spread of the sigma points. A typical value is 10^{-3} . The constant κ is a secondary tuning parameter. Us-

$$\begin{bmatrix} x_1(k+1) \\ x_2(k+1) \\ x_3(k+1) \\ x_4(k+1) \end{bmatrix} = \begin{bmatrix} x_1(k) \\ x_2(k) \\ x_3(k) \\ x_4(k) \end{bmatrix} + T \begin{bmatrix} \frac{B_{\text{effA}}}{A_A u_1(k) + V_{0A}} (Q_A(x_1(k), x_3(k)) - u_2(k) A_A) \\ \frac{B_{\text{effB}}}{A_A(x_{\text{max}} - u_1(k)) + V_{0B}} (Q_B(x_2(k), x_3(k)) + u_2(k) A_B) \\ x_4(k) \\ K \omega_n u_3(k) - 2 \omega_n d_r x_4(k) - \omega_n^2 x_3(k) \end{bmatrix} \quad (18)$$

ally it is chosen as zero. The constant β affects the weight of the first error covariance term. An optimal value is $\beta = 2$ for normally distributed states. The matrix square root in Eq. 5 should be calculated with Cholesky decomposition for computational efficiency.

If the measurement equations in function h are linear, steps 4a and 4b can be simplified. The equations in step 4a reduce to (Welch and Bishop, 2001):

$$\begin{aligned}\hat{\mathbf{y}}_{k+1} &= \mathbf{H} \hat{\mathbf{x}}_{k+1}^- \\ \mathbf{P}_{yy} &= \mathbf{H} \mathbf{P}_{k+1}^- \mathbf{H}^\top + \mathbf{R}_{k+1}\end{aligned}\quad (14)$$

Then step 4b reduces to:

$$\mathbf{P}_{xy} = \mathbf{P}_{k+1}^- \mathbf{H}^\top \quad (15)$$

where \mathbf{H} is a measurement matrix of size $M \times N$.

3.3 Unscented Kalman Filter Implementation for the Test Bed

The online estimation of unknown load variables is possible (An et al., 2008), but not very feasible for FDI purposes because the UKF might compensate a fault by incorrectly estimating the load variables, hence making the fault undetectable. The problem is solved with the inclusion of position and velocity measurements to control vector \mathbf{u} (Chen, 2010). The control vector then becomes:

$$\mathbf{u} = [x, \dot{x}, u_c, p_s] = [u_1, u_2, u_3, u_4] \quad (16)$$

where x is the position, \dot{x} is the velocity, u_c is the valve control signal and p_s is the supply pressure. The position and velocity measurements could also be included to the state vector for filtering.

In the test bed, boom angle was measured and converted to piston position from which velocity was differentiated.

3.3.1 Process Model

The task of the UKF is to estimate pressures p_A and p_B , spool position X_s and spool velocity \dot{x}_s . The reduced-order state vector is thus:

$$\mathbf{x} = [p_A, p_B, x_s, \dot{x}_s]^\top = [x_1, x_2, x_3, x_4]^\top \quad (17)$$

Consequently, the discrete-time state space representation from (Nurmi and Mattila, 2011), Eq. 22, reduces to:

In the GSA in (Nurmi and Mattila, 2011), the effective bulk moduli B_{effA} and B_{effB} were shown to be somewhat influential in transients, so effort was used to correctly identify them. They were found to be dependent on piston position. In particular, B_{effA} was quite small when the piston was completely retracted but gradually grew as the piston extended. The following equations taking the flexible volume of the hoses into consideration gave a good approximation:

$$B_{\text{effA}} = \frac{B_o B_h (A_A u_1(k) + V_{0A})}{(A_A u_1(k) + V_{0A}) B_h + V_h B_o} \quad (19)$$

$$B_{\text{effB}} = \frac{B_o B_h (A_B (x_{\text{max}} - u_1(k)) + V_{0B})}{(A_B (x_{\text{max}} - u_1(k)) + V_{0B}) B_h + V_h B_o}$$

where B_o is the bulk modulus of oil, B_h is the bulk modulus of the hose and V_h is the volume of the hose.

The flow coefficients, shown to be sensitive parameters and treated as constants in the GSA (Nurmi and Mattila, 2011), were not constants but nonlinear functions of spool position. To improve modelling accuracy each flow coefficient was fitted to a third-order polynomial (Muenchhof and Beck, 2008):

$$K_v(x_3) = a_3 x_3^3 + a_2 x_3^2 + a_1 x_3 + a_0 \quad (20)$$

Flow coefficient sample points were obtained off-line by applying nonlinear parameter estimation techniques to step responses of the valve. Fitting a third-order polynomial to the sample points gave the best compromise between accuracy and complexity; see Root Mean Square Errors (RMSE) in Table 2. The fitted polynomials are shown in Fig. 5 with the polynomial coefficients given in Table 10.

In reality, the flow coefficients are also dependent on fluid temperature since the viscosity of the fluid changes with temperature. This modelling was omitted.

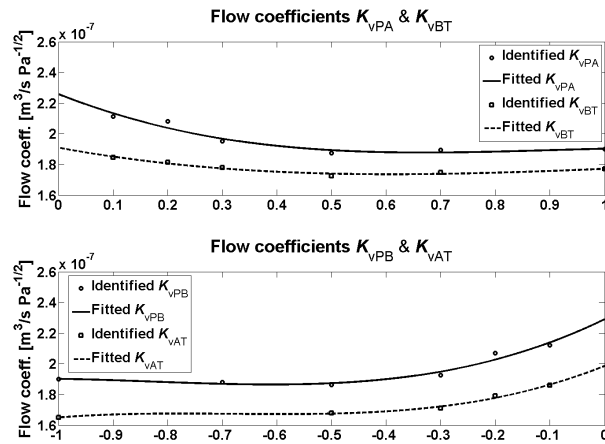


Fig. 5: Flow coefficients of the valve

Table 1: Flow coefficient polynomials

K_{vPA}	$(-5.121 \times 10^{-8} x_3^3 + 1.556 \times 10^{-7} x_3^2 - 1.377 \times 10^{-7} x_3 + 2.256 \times 10^{-7}) * m^3 / (s * Pa^{1/2})$
K_{vPB}	$(9.003 \times 10^{-8} x_3^3 + 2.242 \times 10^{-7} x_3^2 + 1.73 \times 10^{-7} x_3 + 2.291 \times 10^{-7}) * m^3 / (s * Pa^{1/2})$
K_{vAT}	$(1.031 \times 10^{-7} x_3^3 + 2.118 \times 10^{-7} x_3^2 + 1.423 \times 10^{-7} x_3 + 1.986 \times 10^{-7}) * m^3 / (s * Pa^{1/2})$
K_{vBT}	$(-2.371 \times 10^{-8} x_3^3 + 7.573 \times 10^{-8} x_3^2 - 6.588 \times 10^{-8} x_3 + 1.91 \times 10^{-7}) * m^3 / (s * Pa^{1/2})$

Table 2: A comparison of the goodness-of-fits between 1st and 3rd order polynomials

Flow coefficient	Polynomial degree	RMSE [$m^3/s Pa^{1/2}$]
K_{vPA}	1	7.11×10^{-9}
K_{vPA}	3	3.94×10^{-9}
K_{vBT}	1	3.76×10^{-9}
K_{vBT}	3	1.49×10^{-9}
K_{vPB}	1	9.21×10^{-9}
K_{vPB}	3	4.96×10^{-9}
K_{vAT}	1	5.38×10^{-9}
K_{vAT}	3	1.64×10^{-9}

3.3.2 Initialization

The UKF is initialized as follows:

$$\begin{aligned} \mathbf{x}_0 &= [0, 0, 0, 0]^T \\ \mathbf{P}_0 &= \text{diag}([10^{12}, 10^{12}, 10^{-3}, 10^{-3}]) \\ \mathbf{R} &= \text{diag}([10^{10}, 10^{10}]) \\ \mathbf{Q} &= \text{diag}([10^8, 10^8, 10^{-10}, 10^{-10}]) \\ \alpha &= 0.001 \\ \beta &= 2 \\ \kappa &= 0 \end{aligned} \quad (21)$$

where \mathbf{x}_0 is the initial state, \mathbf{P}_0 is the state covariance matrix, \mathbf{R} is the measurement noise matrix and \mathbf{Q} is the process noise matrix.

The tuning parameters α , β and κ were chosen according to existing literature (Wan and van der Merwe, 2000). R was chosen to represent measurement noise. The standard deviations of the pressure sensor readings were roughly 0.1 MPa.

The process noise covariance matrix \mathbf{Q} represents modeling errors. It proved important to find a balance between process and measurement noise. The variances of process noise were chosen slightly smaller than the variances of measurement noise.

The measurement equations were linear, so the algorithm was reduced according to Eq. 14 and 15. The measurement matrix \mathbf{H} was:

$$\mathbf{H} = \begin{bmatrix} 1 & 0 & 0 & 0 \\ 0 & 1 & 0 & 0 \end{bmatrix} \quad (22)$$

3.4 Fault Detection Principles

Pressures A and B residuals were calculated for detecting faults, which was justified on the basis of the GSA results provided in (Nurmi and Mattila, 2011). The residuals $r(k)$ were calculated as follows:

$$r(k) = p(k) - \hat{p}(k) \quad (23)$$

where $p(k)$ and $\hat{p}(k)$ are the measured and estimated pressures, respectively, and k denotes the current time instant. The residuals were averaged within a moving 5-second window to remove the effect of brief estimation errors. The residual average $\mu_r(k)$ was calculated recursively with (Muenchhof and Isermann, 2005):

$$\mu_r(k) = \mu_r(k-1) + \frac{1}{N[r(k) - r(k-N)]} \quad (24)$$

where N , the sample size, was 5000. The recursive formula, although computationally efficient, requires that N samples are stored in memory.

Because the process model cannot be tuned to perfection, a threshold is needed that ensures that the ratio between false alarms (false positives) and undetectable faults (false negatives) is as low as possible. To clarify, the threshold should be constructed in a way that that false alarms are minimized, but at the same time the threshold should as low as possible so that small faults can be detected. Of course to achieve this, the most important factor is the accuracy of the UKF process model.

It is usually enough to use a positive, constant threshold. In this case, the constant positive threshold was not sufficient. A negative threshold was needed so that negative residuals could be used in fault isolation. Also a constant threshold did not work, since the residuals in a faultless situation were larger in chamber A than in B. The reason for this was the load force causing a higher A than B pressure. Consequently, a pressure-dependent threshold was created. A smooth threshold was obtained by averaging both pressures within a moving 5-second window.

Through careful experiments, the following threshold polynomial produced the best results in terms of few false alarms and satisfactory fault detection:

$$t_{\text{pos}}(\mu_p(k)) = 0.012 + 4 \times 10^{-4} \mu_p^2 \quad (25)$$

The unit of the threshold was MPa. The magnitude of the first term was based on the accuracy of the model. The second term ensured that the threshold increased at a suitable rate. The negative threshold was simply $t_{\text{neg}}(\mu_p(k)) = -t_{\text{pos}}(\mu_p(k))$.

3.5 Fault Isolation Patterns

Leakage and valve faults were studied Fig. 6. The leakage faults were divided into ‘External leakage in chamber A’, ‘External leakage in chamber B’, ‘External leakage in chambers A and B’ and ‘Internal leakage’. The valve faults were divided according to relative opening into ‘Stuck to closed position’, ‘Too small an opening’ and ‘Too large an opening’.

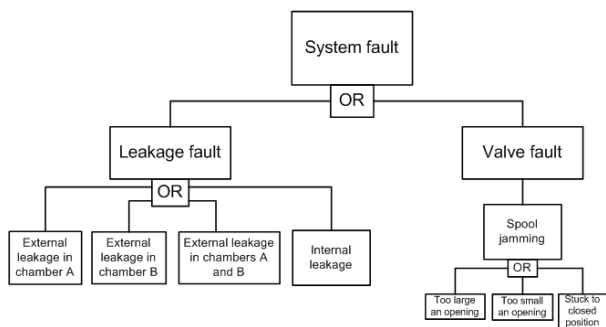


Fig. 6: Fault tree (according to Isermann, 2006, p. 52)

Once a fault was detected, the residuals and other variables were tested against fault patterns that were verified with experiments or simulations to isolate the fault: where \uparrow denotes the crossing of the positive threshold, \downarrow the crossing of the negative threshold, r_{p_A} is the pressure A residual, r_{p_B} is the pressure B residual and u_c is the valve control signal.

For example, an external leakage A causes the pressure A residual to cross the negative threshold ($r_{p_A} \downarrow = 1$), and the residual r_{p_B} to remain within thresholds ($r_{p_B} \uparrow = 0$ and $r_{p_B} \downarrow = 0$). Considering the direction of the residual we could distinguish simultaneous external leakage A and B from internal leakage and from certain valve faults.

The faults where the valve opens too wide or too little can be instantly isolated from internal leakage with a 50 percent probability when both are considered as likely. The possibility of instant detection depends on the test ‘ $p_A > p_B$ ’. For example if the first four binaries of the fault code are 0110, and the fifth, the test ‘ $p_A > p_B$ ’ is false, there is offset in the spool position, so either the valve opened too little or too wide. If the test ‘ $u_c > 0$ ’ is true, the valve opening was too small. If it is false, the valve opening was too large. It is possible to isolate the valve fault when the control signal changes from positive to negative or vice versa by observing whether the residuals cross the opposite thresholds. Internal leakage, on the other hand, is not dependent on the sign of valve control signal.

The rationales behind the patterns are as follows. Consider external leakage A as an example. The GSA (Nurmi and Mattila, 2011) proved that both pressures are sensitive to a chamber A leakage. However, only the residual r_{p_A} crosses the negative threshold, since the pressure differential \dot{p}_A is missing a leakage flow term. The velocity also changes, as shown in the GSA (Nurmi and Mattila, 2011). However, its effect to pressure residuals is minor. A similar description applies to external leakage B and internal leakage. However, in internal leakage faults a leakage is present in both chambers. In one chamber the leakage flow is negative, and in the other it is positive.

When the valve is given a positive control signal and it fails to open as much as it should (fault # 5), the flow rate to chamber A is too small compared to a fault-free situation. Thus the pressure A measurement is smaller than the UKF estimate and consequently the pressure A residual crosses the negative threshold. At the same time, the pressure B residual crosses the positive threshold because the measured B pressure, as a consequence of the restricting action of the smaller notch BT opening, is larger than the estimated B pressure. Similar explanations apply to faults # 6 to 10. In faults # 9 and 10, the valve is completely closed, so the magnitudes of the residuals reveal the cause.

Table 3: Fault patterns for leakage and valve faults

#	Fault	$r_{p_A} \uparrow$	$r_{p_A} \downarrow$	$r_{p_B} \uparrow$	$r_{p_B} \downarrow$	$p_A > p_B$	Large r_{p_A} & r_{p_B}	$u_c > 0$
1	External leakage A	0	1	0	0	0 / 1	0	0 / 1
2	External leakage B	0	0	0	1	0 / 1	0	0 / 1
3	Internal leakage A→B	0	1	1	0	1	0	0 / 1
4	Internal leakage B→A	1	0	0	1	0	0	0 / 1
5	Spool jamming, too small an opening 1	0	1	1	0	0 / 1	0	1
6	Spool jamming, too small an opening 2	1	0	0	1	0 / 1	0	0
7	Spool jamming, too large an opening 1	1	0	0	1	0 / 1	0	1
8	Spool jamming, too large an opening 2	0	1	1	0	0 / 1	0	0
9	Spool jamming, stuck to closed position 1	0	1	1	0	0 / 1	1	1
10	Spool jamming, stuck to closed position 2	1	0	0	1	0 / 1	1	0

4 Results

Experimental results for detecting and isolating leakages are given in Section 4.1. In Section 4.2, the detection and isolation of valve faults is studied with simulations.

4.1 Experimental Results

The experimental results consist of external leakage A, external leakage B, simultaneous external leakage A and B, and internal leakage. The valve was controlled with fairly random control signals Fig. 7.

In the residual figures, the black vertical line shows the time when the fault was added, the solid red line the residuals, and the dashed black lines the thresholds.

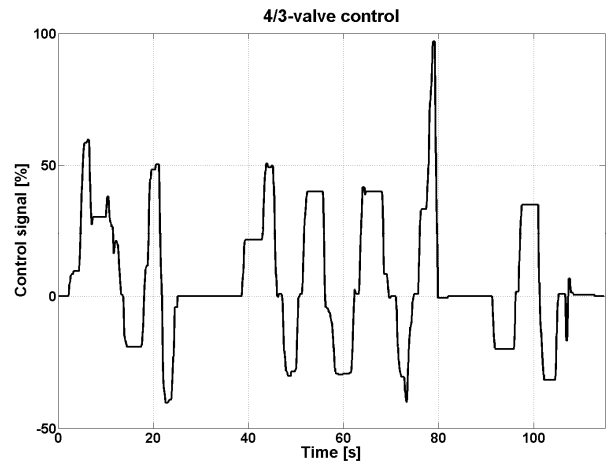


Fig. 7: Example control signal to the 4/3-directional valve that was used in the external leakage B experiment

4.1.1 External Leakage in Chamber A

The external leakage A was added to the system at around the 35th second. The evolution of pressure A and pressure B measurements and estimates are given in Fig. 8. The estimates are in blue and the measurements in red colour.

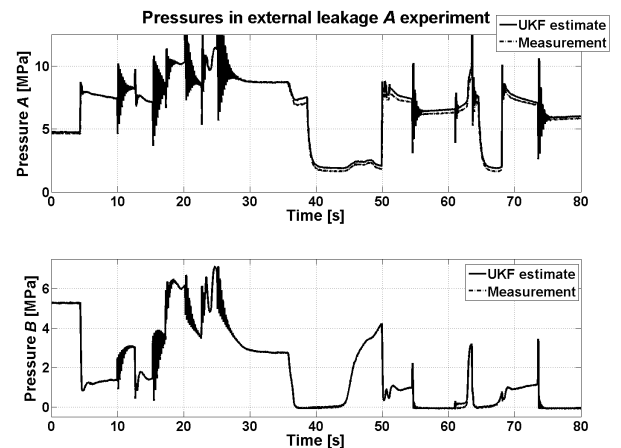


Fig. 8: The evolution of pressure A and B estimate and measurement

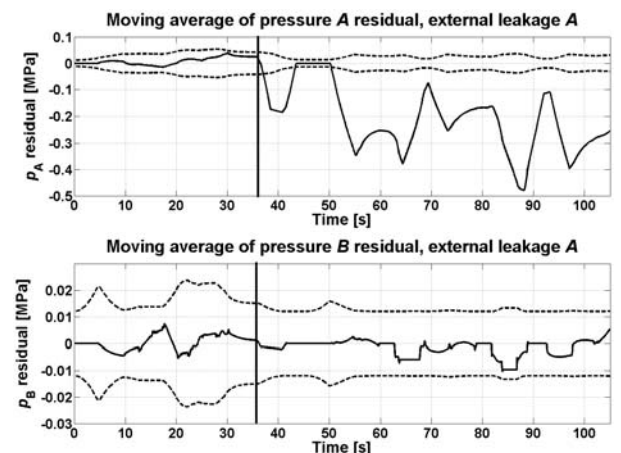


Fig. 9: Pressure residuals (in solid red) with a varying external leakage in chamber A of average 1.40 l/min. The thresholds are the dashed black lines

Between the 35th and 50th second the difference between the pressure A measurement and its estimate is not clear-cut. From the 50th second onwards, the difference becomes clear and is indistinguishable between pressure B measurements and estimates Fig. 8.

The external leakage A was detectable two seconds later when the pressure A crossed the negative threshold at -0.04 MPa, see Fig. 9. Therefore, according to the fault patterns in Table 3, the fault could be isolated as external leakage A (fault # 1). The magnitude of the residual indicates that the fault is severe. According to flow measurements, a detectable external leakage was close to 0.40 l/min or 10 % of the flow rate passing the valve.

The residuals were momentarily decreased to zero since there were some non-fault related discrepancies between measurements and UKF estimates when the pressure B was close to zero or the boom angle was zero. Excluding these situations, the scheme worked.

4.1.2 External Leakage in Chamber B

The external leakage B was added to the test bed at around the 30th second. The fault was detectable a few seconds later when pressure B crossed the negative threshold, as illustrated in Fig. 10.

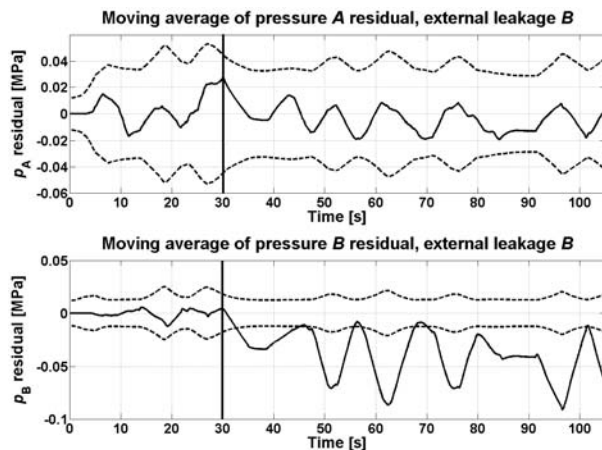


Fig. 10: Pressure residuals with an external leakage in chamber B with average 0.50 l/min

According to fault patterns in Table 3, the fault could be isolated as external leakage B (fault # 2). As pressure B was smaller than pressure A, the thresholds for B residuals could be considerably smaller allowing for a smaller leakage to be detected. At the time of detection, the threshold was -0.015 MPa and the minimum detectable leakage approximately 0.17 l/min, or 5 % of the flow through the 4/3 directional valve, significantly smaller than the detectable leakage from chamber A. The leakage varied between 0.14 l/min and 1 l/min (see the varying magnitude of residual), but on average it was 0.50 l/min.

When the pressure A residual approached the threshold, the threshold increased, proving that the thresholds were indeed pressure dependent and so the proposed adaptive threshold worked.

4.1.3 Simultaneous External Leakage in Chambers A and B

An external leakage A and B were simultaneously introduced to the test bed at the 18th second, as shown in Fig. 11. The external leakage A was detectable only a second later, but the external leakage B took over 30 seconds to detect. The reason for the slow detection was the decreased pressure A that decreased pressure B causing a minor leakage from chamber B. The leakage in chamber B rose to 0.18 l/min before the actual detection of the fault, but a short leakage peak of this magnitude could not be detected. The leakage peaked at 0.52 l/min (average 0.30 l/min) and 0.60 l/min (average 0.34 l/min) at 50 and 65 seconds, and at those instants the threshold of residual B was clearly crossed.

An external leakage A of 0.50 l/min could be detected as that was the leakage magnitude at the time of detection. The leakage averaged at 1.6 l/min between 40 and 70 seconds, but the residual during this period was well over the threshold.

The isolation follows the patterns in Table 3. For the reasons in Section 4.1.1, the residuals were momentarily forced to zero.

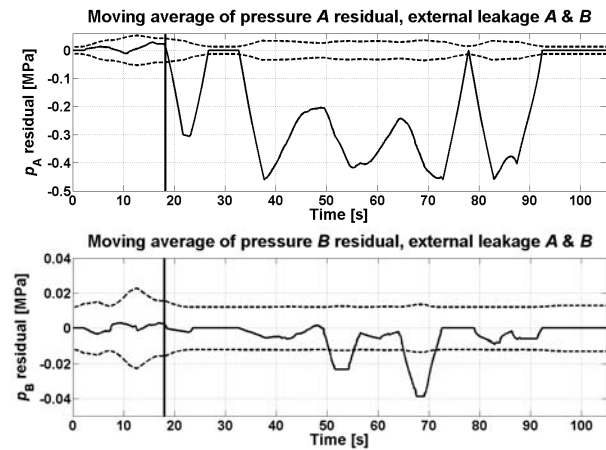


Fig. 11: Pressure residuals with an external leakage in chambers A and B. An external leakage A of 11 % (average 1.60 l/min) and an external leakage B (average 0.30 l/min) of 5 % of flow through the valve were detectable

4.1.4 Internal Leakage

The internal leakage was added to the test bed at the 30th second, as shown in Fig. 12. The positive threshold of pressure B residual was crossed roughly three seconds sooner than the negative of pressure A residual. The leakage varied between 0.35 l/min and 2 l/min, and on average it was 0.94 l/min. During the experiment when the leakage dropped significantly below the average, the thresholds remained in the fault range, showing that an internal leakage of below 0.50 l/min could be detected, or a leakage in the range of 5 - 10 % of the flow passing the 4/3-directional valve.

The isolation of the internal leakage was not entirely straightforward following Table 3. Since $p_A > p_B$ was always true, at the time of detection the fault was either an internal leakage (fault # 3), or the spool had opened too wide (fault # 7 and # 8) or too little (fault # 5 and # 6). As time progressed, the residuals did not cross the

other threshold as the control signal changed. Therefore the fault could be isolated as internal leakage.

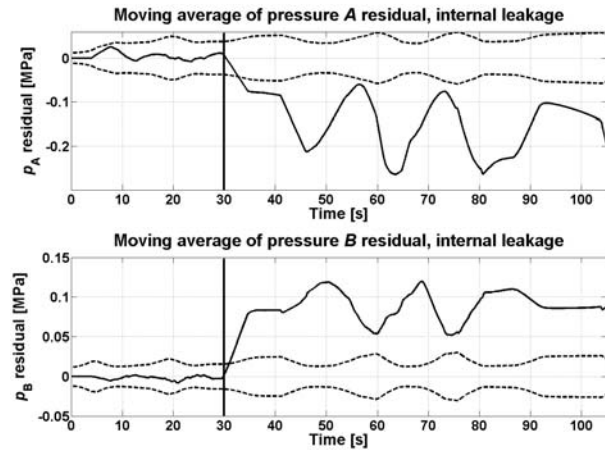


Fig. 12: Pressure residuals with an internal leakage of average 0.94 l/min

4.2 Simulation Results

The accuracy of the UKF process model in simulations guaranteed that the residuals stayed close to zero in a faultless situation. For consistency the adaptive threshold was used in simulations. White, normally distributed noise was added to simulation pressures so that they bore more of a resemblance to experimental measurements. In addition, the UKF parameters were retuned. The process noise variances of pressures were reduced to 10^4 Pa^2 and the measurement noise variances to 10^5 Pa^2 . The 4/3 directional valve control signal used in simulations is shown in Fig. 13.

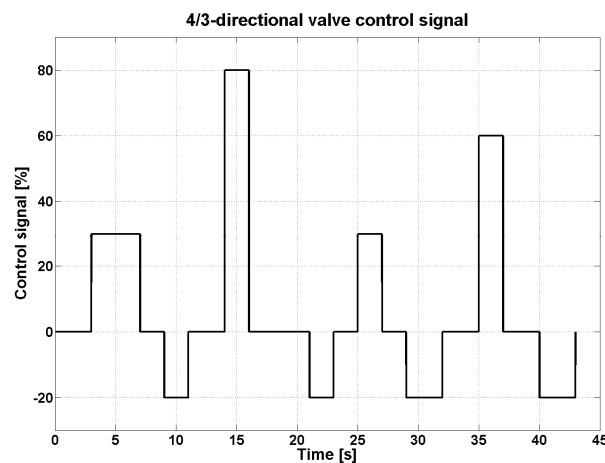


Fig. 13: The valve control signal in simulation experiments

4.2.1 Too Small Valve Opening

The ‘too small valve opening’ fault was introduced to the system at the 35th second, as is illustrated in.

After a second, the fault was detected but could not be immediately isolated since pattern was similar to internal leakage (# 3). Once both residuals, as a consequence of the valve control signal change, crossed the other threshold at approximately the 42th second, the fault could be isolated as too small valve opening fault (# 5 and 6).

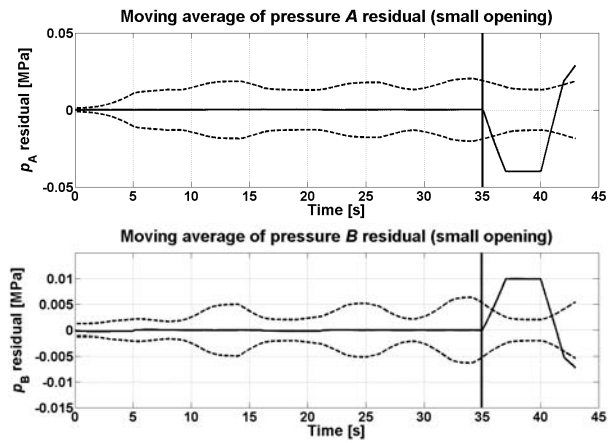


Fig. 14: The spool jams so that the opening is too small

4.2.2 Too Large Valve Opening

The fault ‘too large valve opening’ (# 7 and 8) was added to the system at the 35th second, as shown in Fig. 15. The residual behaviour was reversed compared to fault case ‘too small valve opening’. Hence the isolation was possible immediately after detection.

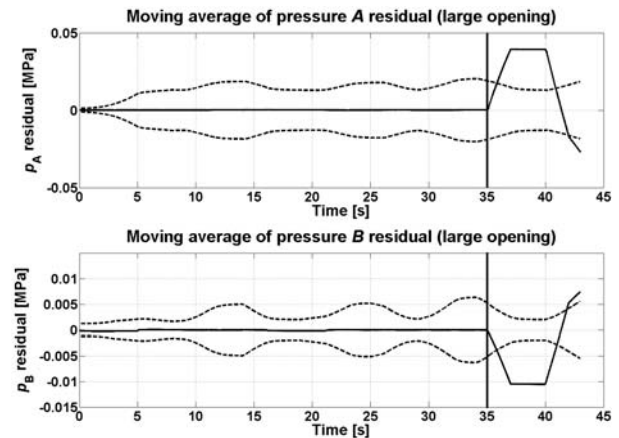


Fig. 15: The spool jams so that the opening is too large

If the internal leakage would have occurred from chamber B to A, this fault could have been isolated, although not instantly following detection.

4.2.3 Valve gets Stuck to Closed Position

At the 35th second, the valve spool got stuck to closed position, shown in Fig. 16.

The residual behaviour was similar to internal leakage (# 3), except that the residuals crossed the opposite threshold when the valve control signal was reversed at the 40th second. The magnitudes of the residuals revealed the cause as being a closed valve (# 9 and 10).

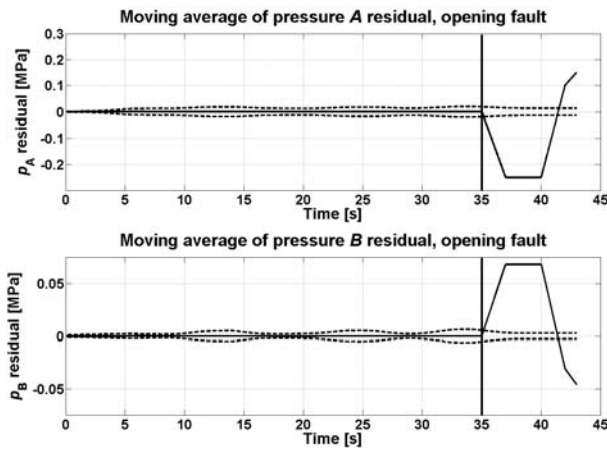


Fig. 16: The valve spool stuck to closed position

5 Conclusions

In this paper a real-time scheme based on a reduced-order Unscented Kalman Filter (UKF) for detecting and isolating leakage and valve faults from a generic valve-controlled hydraulic cylinder driving a manipulator joint in varying loading conditions was devised and applied to a hydraulic boom test bed. The method is a practical load-independent solution for detecting and isolating especially leakages. In the paper, a comprehensive set of fault patterns were presented, and an adaptive threshold facilitating fault detection was devised. The basis for this work was founded in (Nurmi and Mattila, 2011), where a Global Sensitivity Analysis (GSA) of the test bed was carried out. The results of the analysis were used in this paper, showing that GSA facilitates a systematic and verified approach to model-based condition monitoring. The usefulness of GSA increases with more complicated nonlinear models.

The fault patterns were verified with simulation and experimental studies. The studies, with leakage patterns verified experimentally, showed the possibility of distinguishing external leakage A and B, and simultaneous external leakage A and B from valve faults (spool jamming to too large an opening, to too small an opening and stuck to closed position).

The lowest detectable external leakage was 0.17 l/min, but it varied between experiments. The pressure residuals alone were not enough to distinguish internal leakage and valve faults, so information from the sign of the control signal and the larger chamber pressure were used. The control signal test meant that the time from fault detection to isolation was considerably long in some valve opening or internal leakage fault cases. The fault patterns for those two different faults were found similar, and hence very difficult to distinguish.

The fault-to-isolation time could be shortened and the fault patterns could be expanded by utilizing a spool position measurement. This measurement, however, is not usually available. Moreover, the scheme already requires multiple measurements, and increasing measurements would increase the probability of sensor failures. The required measurements, however, are:

cylinder chamber pressures A and B, supply pressure, valve control signal, piston position or boom angle, and piston velocity or boom angular velocity measurement. If a separate velocity measurement is not available, the velocity could be differentiated from position.

The scheme will be extended to mobile valves using position and velocity sensors more suitable for application domain specific environmental conditions in the future.

Nomenclature

H	Measurement matrix	[-]
K	Kalman gain	[-]
P	Posteriori state covariance matrix	[-]
P[*]	Priori state covariance matrix	[-]
P_{xy}	Cross-covariance matrix	[-]
P_{yy}	Measurement covariance matrix	[-]
Q	Process noise covariance matrix	[-]
R	Measurement noise covariance matrix	[-]
<i>r</i>	Residual	[MPa]
<i>t_{pos,neg}(μ_p)</i>	Positive and negative threshold polynomial	[MPa]
x	State vector	[-]
\hat{x}	State estimate vector	[-]
$\tilde{x}^{(i)}$	Sigma point vector	[-]
y	Measurement vector	[-]
μ_p	Pressure average	[MPa]
v	Measurement noise vector	[-]
w	Process noise vector	[-]

Subscripts:

k Discrete time instant

Acknowledgements

This work was funded by the Academy of Finland under the project 133273, Sensor network based intelligent condition monitoring of mobile machinery. The authors gratefully acknowledge the Academy of Finland for the financial support.

References

- An, L. and Sepehri, N.** 2008. Leakage fault detection in hydraulic actuators subject to unknown external loading. *International Journal of Fluid Power*, volume 9, issue 2, August 2008, pp 15 - 25.
- Chen, L.** 2010. *Model-based fault diagnosis and fault-tolerant control for a nonlinear electro-hydraulic system*. Ph.D. Thesis. University of Kaiserslautern.
- Goharrizi, A. Y., Sepehri, N.** 2010a. A wavelet-based approach to internal seal damage diagnosis in hydraulic actuators. *IEEE Trans. on Ind. Electron.*, Vol. 57, No. 5, pp. 1755 - 1762.

- Goharrizi, A. Y., Sepehri, N. and Wu, Y.** 2010b. A wavelet based approach for diagnosis of internal leakage in hydraulic actuators using on-line measurements. *International Journal of Fluid Power*, Vol. 11, No.1, pp. 61 - 69.
- Goharrizi, A. Y., Sepehri, N. and Wu, Y.** 2011. A wavelet-based approach for online external leakage diagnosis and isolation from internal leakage in hydraulic actuators. *International Journal of Fluid Power*, Vol. 12, No. 2, pp. 37 - 47.
- Isermann, R.** 2006. *Fault-diagnosis systems, an introduction from fault detection to fault tolerance*. Springer-Verlag Berlin Heidelberg. p. 475.
- Julier, S. J., Uhlmann, J. K. and Durrant-Whyte, H. F.** 1995. A new approach for filtering nonlinear systems. *Proceedings of the American control conference*, Seattle, Washington, 1995, pp. 1628 - 1632.
- Julier, S. J. and Uhlmann, J. K.** 1997. A new extension of the Kalman filter to nonlinear systems. *Proceedings of AeroSense, the 11th international symposium on aerospace/defence sensing, simulation and controls*, pp. 182 - 193.
- Le, T. T., Watton, J. and Pham, D. T.** 1997. Fault classification of fluid power systems using a dynamics feature extraction technique and neural networks, *Proc. Instn. Mech. Engrs*, Vol. 212, Part I, pp. 87 - 96.
- Muenchhof, M. and Isermann, R.** 2005. Comparison of change detection methods for a residual of a hydraulic servo axis. *Proceedings of the 16th IFAC world congress, international federation of automatic control*, Czech Republic.
- Muenchhof, M. and Beck, M.** 2008. Model adjustment and multi-model based fault diagnosis for hydraulic servo axis. *Proceedings of the 17th world congress, the international federation of automatic control*, Seoul, Korea.
- Nurmi, J. and Mattila, J.** 2011. Detection and isolation of leakage and valve faults in hydraulic systems in varying loading conditions, Part 1: Global Sensitivity Analysis. *International Journal of Fluid Power*, Vol. 12, No. 3.
- Saltelli, A., Ratto, M., Andres, T., Campolongo, F., Cariboni, J., Gatelli, D., Saisana, M. and Tarantola, S.** 2008. *Global sensitivity analysis: the primer*. John Wiley & Sons. p. 292.
- Sepasi, M. and Sassani, F.** 2010. On-line fault diagnosis of hydraulic systems using unscented Kalman filter. *International journal of control, automation, and systems*, Vol. 8, Issue 1, 2010, pp. 149 - 156.
- Simon, D.** 2006. *Optimal state estimation: Kalman, H_∞ , and nonlinear approaches*. Wiley-Interscience. p. 526.
- Tan, H. and Sepehri, N.** 2002. Parametric fault diagnosis for electrohydraulic cylinder drive units. *IEEE Trans. Industrial Electronics*, Vol. 49, pp. 96 - 106.
- Wan, E. A. and van der Merwe, R.** 2000. The Unscented Kalman Filter for nonlinear estimation. *Proceedings of IEEE adaptive systems signal processing, communication and control symposium*, October 2000, pp. 153 - 158.
- Watton, J.** 2007. *Modelling, monitoring and diagnostic techniques for fluid power systems*. Springer-Verlag London Ltd. p. 360.
- Welch, G. and Bishop, G.** 2001. *An introduction to the Kalman filter*. Department of computer science, University of North Carolina, Chapel Hill, TR95-041.



Jarmo Nurmi

Jarmo Nurmi graduated with a B.Sc. and M.Sc. in hydraulic engineering in 2009 and 2011, respectively, at the Tampere University of Technology (TUT). He is currently working as a researcher at TUT in the department of Intelligent Hydraulics and Automation (IHA). His research interests are mobile hydraulics and condition monitoring.



Jouni Mattila

Professor, Dr. Tech. Jouni Mattila received M.Sc. (Eng.) in 1995 and Dr. Tech 2000 both from TUT. He is a TUT program manager in ITER Remote Handling robotics maintenance projects. He is a coordinator of Marie Curie Initial training Network program: PURESAFE with 15 PhD-students across the EU. His research interests include machine automation and preventive maintenance, and fault-tolerant control system development for advanced machines utilizing lean systems engineering framework.